# Determination of the crystal-field splitting of the math xmlns="http://www.w3.org/1998/Math/MathML">mrow>mn >4/mn>msup>mrow>mi>f/mi>/mrow>mn>1/mn>/msup >/mrow>/math> state in samarium-alloyed cerium hexaboride

Gan Zhao, Huayao Li, Wenting Lin, Quan Ren, Jonathan Denlinger, Yi-De Chuang, Xiaoqian Zhang, L. Andrew Wray, and Lin Miao

Phys. Rev. B **107**, 245149 — Published 30 June 2023

DOI: 10.1103/PhysRevB.107.245149

# Determination of crystal field splitting of $4f^1$ state in the samarium-alloyed cerium hexaboride

Gan Zhao,[1] Huayao Li,[1] Wenting Lin,[1] Quan Ren,[1] Jonathan Denlinger,[2] Yi-De Chuang,[2] Xiaoqian Zhang,[3] L. Andrew Wray,[4,*] and Lin Miao[1,†]

[1]*Key Laboratory of Quantum Materials and Devices of Ministry of Education, School of Physics, Southeast University, Nanjing 211189, China*
[2]*Advanced Light Source, Lawrence Berkeley National Laboratory, Berkeley, California 94720, USA*
[3]*International Quantum Academy, Shenzhen 518048, China*
[4]*Department of Physics, New York University, New York, New York 10003, USA*

(Dated: June 21, 2023)

The cerium hexaboride and its alloyed compounds are strongly correlated materials, hosting many-body hidden order or non-trivial band topology. The fine electronic structure of the Ce-$4f^1$ state, derived from the spin-orbit coupling and the crystal electric field splitting (CEF), plays a vital role in forming the exotic quantum state in the Ce-based compounds. By using the high-resolution resonant inelastic X-ray scattering technique, we determined the fine electronic excitation energies of the Ce-$4f^1$ state in the Kondo material $Ce_{0.3}Sm_{0.7}B_6$. The extracted energy levels show an overall consistency with other scattering techniques, except that CEF splitting in the total angular momentum $J = 7/2$ state is identified to be $(89.5 \pm 1)$ meV, clearly larger than the value of 82 meV drawn from Raman spectroscopy. A detailed discussion is made to reconcile the mismatch. This work provides key information on the Ce-$4f^1$ orbital in $CeB_6$, which would also put a constraint on the related theoretical model, help to address the challenges for theoretical dealing with many-body correlation in Ce-$4f^1$ compounds.

## I. INTRODUCTION

The Ce-based compounds have been intensively studied due to its many-body interaction and the intertwined coupling between different degrees of freedom[1–6]. The stable trivalent Ce ion has an outer shell of $4f^1$. The strong spin-orbit coupling (SOC), high susceptibility to ordered magnetism, and intrinsic Kondo effect within the Ce $4f^1$ state make its compounds a fertile land of electronic correlation and quantum criticality[7, 8]. For instance, Ce-based materials like $CeCu_2Si_2$ and $CeCoIn_5$ are archetypical heavy fermion superconductors[9–11]. The Ce $4f^1$ state also dominates dense Kondo behavior in $Ce_xLa_{1-x}Cu_6$ [12, 13] and $Ce_xLa_{1-x}Ni_2Ge_2$ [14]. Among these correlated materials, $CeB_6$ and its alloyed derivatives like $Ce_{1-x}La_xB_6$ attract particular interest due to their unique properties[15–19]. The $CeB_6$ possesses a cubic lattice under the space group of *Pm3m*. The Ce atoms form the frame of a cube which is centered by an octahedral ($O_h$) boron cage (Fig. 1(a)). The Ce-site can be substituted with other metallic lanthanides like La/Sm/Eu, transforming it to a different quantum phase without altering the crystal structure[20–23]. $CeB_6$ has been found to host the "hidden order" at the temperature between 2.4 K and 3.2 K, which is proposed as a result of the magnetic multipolar effect but is still under debate[24–26]. Despite strong evidence for the existence of the many-body quantum order, recent work reported that substituting Ce with Sm could achieve non-trivial topology in the $Ce_{1-x}Sm_xB_6$ (x > 0.5), which is known as a topological Kondo system[27, 28].

No matter the hidden order or the topological Kondo phase, those exotic properties of $CeB_6$ and its alloyed compounds strongly rely on the energy levels in the vicinity of the Fermi level and the associated ground state symmetries[28, 29]. Massive efforts have been taken to determine the ground state of Ce-$4f^1$[30, 31], and an overview can be achieved (Fig. 1(b)). The strong SOC split the $4f^1$ state into $4f_{7/2}$ and $4f_{5/2}$, in which the $4f_{5/2}$ is ∼270 meV lower in energy[32]. Within the crystal electric field (CEF) of $O_h$ symmetry, the six-fold degenerate $4f_{5/2}$ states are further split into different symmetries of $\Gamma_8$ and $\Gamma_7$. Neutron scatterings and X-ray spectroscopy studies have claimed the CEF in $4f_{5/2}$ as ∼50 meV, and it is now widely acknowledged that quadruplet $\Gamma_8$ is the ground state after a long debate[8, 33]. There are also first-principle calculations aiming to reveal the splitting within the Ce-$4f_{7/2}$ under various CEF symmetries, suggesting an energy hierarchy of $\Gamma_6'$, $\Gamma_8'$, and $\Gamma_7'$ symmetries and their relative energy spacing of ∼100 meV (under tetragonal lattice)[30]. However, most experimental studies focus on the lower branch ($J = 5/2$) of the SOC split $4f^1$ state[8, 20, 29, 34], and the direct measurement of the CEF splitting in an upper branch ($J = 7/2$) of $CeB_6$ has rarely been reported. The only experimental work based on Raman spectroscopy claims the CEF split of 82 meV in $J = 7/2$ state, leading to a discrepancy between the experiment and numerical calculation[35]. To resolve the disputed results, we studied the $4f^1$ orbital's energy hierarchy in $Ce_{0.3}Sm_{0.7}B_6$ by using high-resolution resonant inelastic X-ray scattering (RIXS). The very fine CEF split electronic structures within the $J = 7/2$ and $J = 5/2$ states are depicted. The CEF split energy scale of $J = 7/2$ is discovered to be (89.5

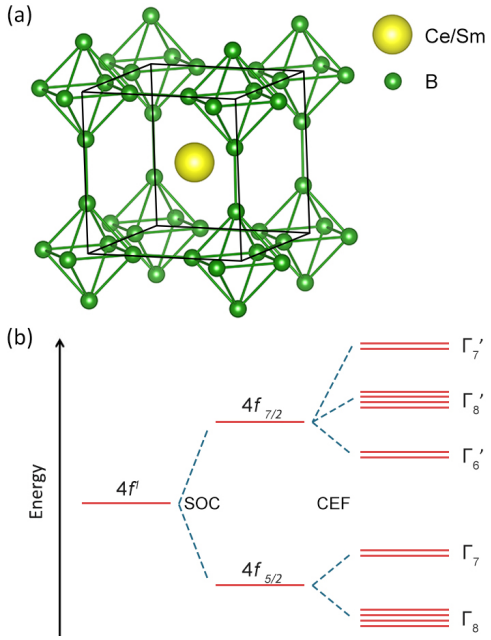


FIG. 1. (a) Ctystal structure of $CeB_6$. (b) Schematic diagram of $Ce^{3+}$ $4f^1$ energy levels. The $4f^1$ orbital is split into two states $4f_{7/2}$ and $4f_{5/2}$ by spin-orbit coupling (SOC). In the crystal electric field (CEF), the $J = 5/2$ states are split into two symmetries $\Gamma_8$ and $\Gamma_7$ , correspond to the 4- and 2-fold degeneracy, and the $J = 7/2$ states are split into three symmetries $\Gamma_7'$, $\Gamma_8'$ and $\Gamma_6'$ which are with 2-, 4- and 2-fold degeneracy respectively.

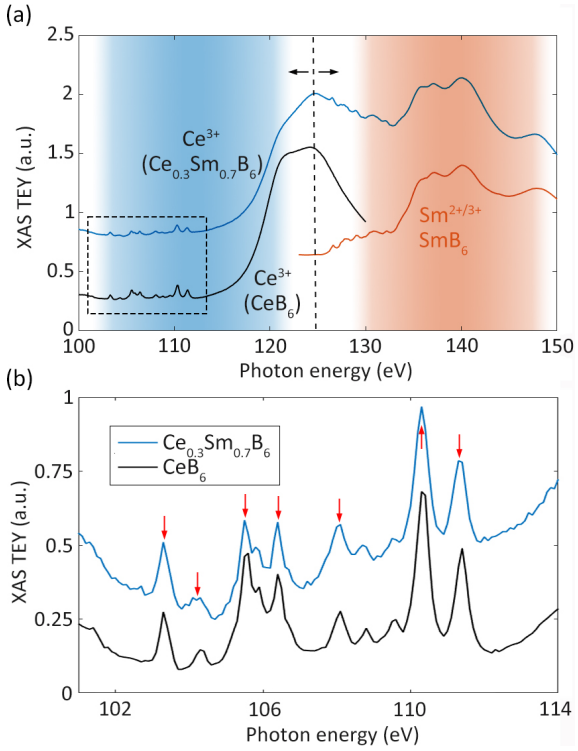


FIG. 2. (a)The $N$-edge XAS on $Ce_{0.3}Sm_{0.7}B_6$ (blue curve), which is compared with the $N$-edge XAS of pristine $CeB_6$ (black curve, shaded with blue) and pristine $SmB_6$ (red curve, shaded with red). (b) The pre-edge fine peaks of Ce-XAS at $h\nu < 114$ eV are compared between the $CeB_6$ and $Ce_{0.3}Sm_{0.7}B_6$. The incident photon energies selected for the following RIXS measurements are marked by the vertical arrows.

$\pm$ 1) meV, which is larger than previously reported. Our work put a well-defined constraint on further theoretical treatment, a step forward to understanding the strongly correlated effect within the Ce-base compound.

## II.EXPRIMENT

The high-resolution X-ray absorption spectroscopy (XAS) and RIXS measurements were both performed at the beamline 4.0.3 endstation (MERIXS) at the Advanced Light Source (ALS). The incident photon energy was tuned between 100 eV to 150 eV to cover the $N_{4,5}$-edge ($4d^{10}$ $4f^n$ to $4d^9 4f^{n+1}$ transition) of Ce or Sm. The total electron yield (TEY) mode was used in the XAS. To gain a good signals' statistics, the RIXS experiment was performed with the $\pi$-polarized incident photons. The $Ce_{0.3}Sm_{0.7}B_6$ samples are with high crystalline qualities, same as the ones in the earlier study[27, 28]. Alloying with Sm makes $Ce_{0.3}Sm_{0.7}B_6$ to be well cleaved, generating high-quality data under the ultraviolet RIXS (see supplementary Fig. S1 [36]). Large single crystals of $Ce_{0.3}Sm_{0.7}B_6$ were cleaved and measured at low temperature (20 K), meanwhile maintained at an ultra-high vacuum with pressure of approximately $3\times10^{-10}$ Torr.

## III.RESULTS AND DISSCUSIONS

The $N_{4,5}$-edge XAS spectrum of the $Ce_{0.3}Sm_{0.7}B_6$ is shown in Fig. 2(a), which is also compared with the XAS of pristine $CeB_6$ and $SmB_6$. Actually, the overall spectrum is a composite of the $N$-edge XAS of both Ce and Sm. Unlike the main absorptive peak which is easily affected by the Fano resonance, the pre-edge peaks are not susceptible to Fano resonance but highly sensitive to the valence state [37]. Through scrutinizing the fine pre-edge peaks at around 110 eV, one could see the pre-edge peaks are almost identical between $CeB_6$ and $Ce_{0.3}Sm_{0.7}B_6$, indicating the trivalent nature of Ce in the $Ce_{0.3}Sm_{0.7}B_6$ (Fig. 2(b)). This confirms that alloying with Sm would not change the valence state of Ce, and vice versa. Meanwhile, atomic multiplets simulation agrees that pre-edge peaks of Ce locates well below $h\nu = 115$ eV, excluding the multiplet states from divalent and trivalent Sm (see supplementary Fig. S2 [36]). The distinct separation of energy between the Ce $N$-edge and Sm $N$-edge provides an excellent opportunity to study the inelastic excitations of Ce without the inclusion of signals from Sm.

It is known that $N$-edge excitation of lanthanide metal

gives rise to a large cross-section for the inelastic X-ray scattering[39, 40]. The first $N$-edge RIXS study on Ce-based compound was reported decades ago, but with very limited energy resolution, and the sub-eV fine inelastic emission is not clearly identified[41, 42]. The remarkable improvement of the energy resolution in RIXS now gives chances to detect fine excitations. Fig. 3(a) shows the Ce $N$-edge RIXS as the dependence of incident photon energies. No matter whether the incident photons locate at the pre-edge fine peaks (from 102 eV to 112 eV) or at the main peaks with higher excitation energy (> 122 eV), their inelastic emissions remain almost constant in energy, in spite of the variation of intensities. The detailed photon emission line-profiles are shown in Fig. 3(b), from where two bunches of excitation peaks can be observed at the lower and higher excitation energy. In the low-energy regime, to the very nearby of the elastic peak, there exists an inelastic emission with a fitted energy loss of ∼50 meV, namely peak 2 (Fig. 3(d)). This excitation recalls previously accounted CEF split energy between quadruplet $\Gamma_8$ and doublet $\Gamma_7$ in the $J = 5/2$ state, which was reported as 60 meV (photoemission[43]), 46 meV (neutron scattering[8]) and 47 meV (Raman scattering[8]). Therefore the peak 2 should be attributed to the CEF excitation from $\Gamma_8$ and $\Gamma_7$. Other relatively weak excitations above 270 meV could be found by looking into the regime with higher energy loss (Fig. 3(c)). This separated energy of 270 meV is coincident with the spin-orbit splitting in the $4f^1$ states[32], which indicates those excitations are spin-orbital excitations by flipping the spins from the $J = 5/2$ to $J = 7/2$ states (see Fig. 1).

As we discussed, intensive efforts have been made to understand the low-energy excitations in the $CeB_6$, but excitation with higher energy has seldom been reported and less discussed. Instead of three energy levels of symmetries ($\Gamma_6'$, $\Gamma_8'$ and $\Gamma_7'$) predicted by the calculation, there seem to be only two peaks in the upper branch from RIXS data (Fig. 3(c)), which is intriguing. The separation of the two peaks is approximately 80 meV, which fits precisely with CEF separation in the Raman experiment but lacks an excitation peak observed before. Assuming $\Gamma_8'$ and $\Gamma_6'$ of $J = 7/2$ states are located too close together could interpret the two excitation peaks in the $J = 7/2$ states. If so, the tiny gap between $\Gamma_8'$ and $\Gamma_6'$ might not be easily distinguished, and only one merged large peak can be detected due to the limited apparatus energy resolution (∼15 meV). Then, a detailed fitting of the upper branch excitations with two peaks is shown in Fig. 4(a-c). The overall fitting quality is acceptable, despite possibly missing some spikes around the two main peaks. The extracted CEF split energy from the dual-peak fitting within $J = 7/2$ is approximately 77 meV, which is smaller than the result of 82 meV from Raman scattering. However, by analyzing the fitting details, one could find that the full width at half maximum (FWHM) value of peak 3 ($\Gamma_8' + \Gamma_6'$) is extraordinarily large, even

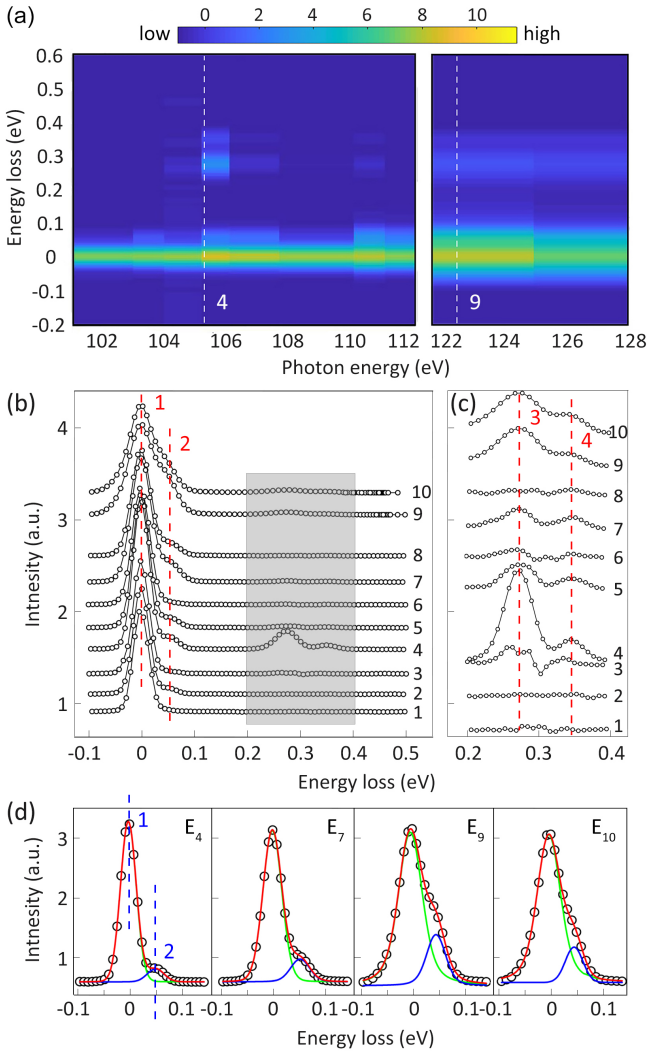


FIG. 3. (a) Ce $N$-edge RIXS map is displayed as a function of the incident photon energy and the energy loss of the scattered photon. (b) The RIXS spectra sliced from the maps at ten different incident photon energies (h$\nu$ = 101.4 eV, 103.3 eV, 104.3 eV, 105.5 eV, 106.4 eV, 108 eV, 110.4 eV, 111.4 eV, 122.2 eV and 125 eV which labeled from $E_1$ to $E_{10}$), in which $E_4$ = 105.5 eV and $E_9$ = 122.2 eV are marked by the white dashed line in (a)). The elastic peak ($\Gamma_8$ and its nearby inelastic peak ($\Gamma_8$) to $\Gamma_7$)) are marked by dashed vertical lines. (c) Magnifying the weak inelastic peaks by zooming in the grey-shaded rectangle in (b). (d) The elastic and inelastic emission of the $J = 5/2$ states from the RIXS curves with good data statistics ($E_4$ = 105.5 eV, $E_7$ = 110.4 eV, $E_9$ = 122.2 eV, and $E_{10}$ = 125 eV) are fitted by two peaks. Black circles are experimental data and red curves are cumulative peaks' fitting results.

twice as its counterpart in peak 4 ($\Gamma_7'$), as shown in Fig. 4(b). Although the four-fold degeneracy of quadruplet $\Gamma_8'$ naturally bears a broadened excitation peak than the double-degenerate $\Gamma_7'$, the dispute cannot be reconciled because the second order split within $\Gamma_8'$ and $\Gamma_7'$ is sub-meV (∼10 K) and it would not profoundly impact the

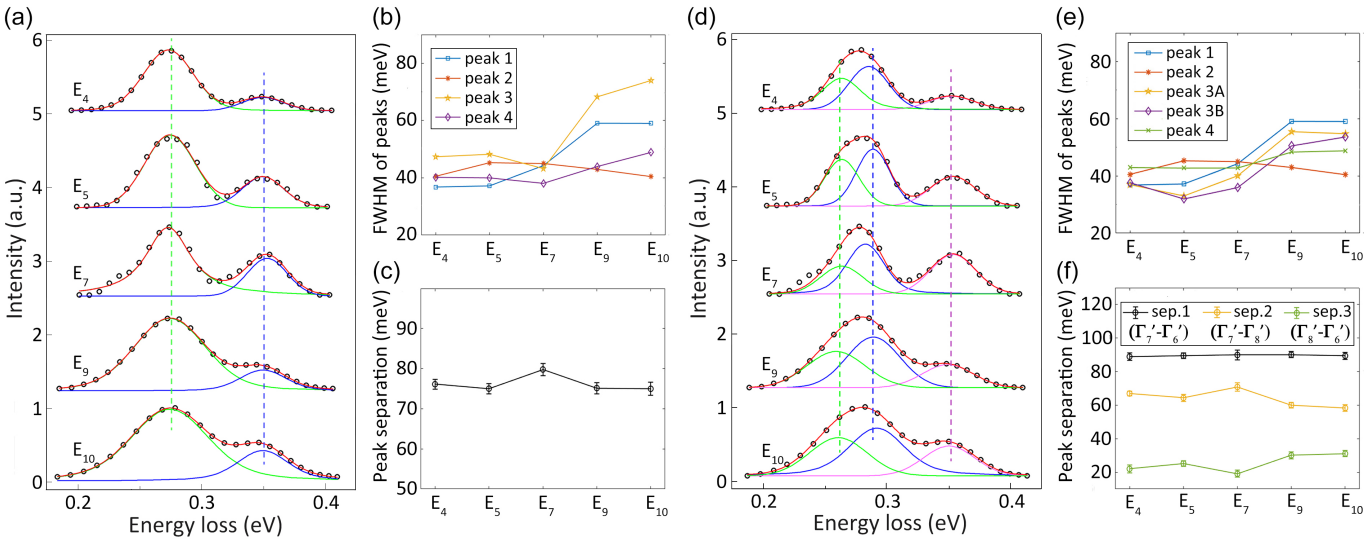


FIG. 4. (a) The inelastic emission of the $J = 7/2$ states from the RIXS curves with good data statistics ($E_4 = 105.5$ eV, $E_5 = 106.4$ eV, $E_7 = 110.4$ eV, $E_9 = 122.2$ eV, and $E_{10} = 125$ eV) are fitted by two peaks. Black circles are experimental data and red curves are cumulative peaks' fitting results. (b) The FWHM values of the fitted peaks extracted from (a) and two fitted peaks in the $J = 5/2$ state. The four peaks represent the elastic peak (peak 1) and the excitation from the ground state to $\Gamma_7$ (peak 2), $\Gamma_6'$+$\Gamma_8'$ (peak 3), and $\Gamma_7'$ (peak 4). (c) The total CEF split within the $J = 7/2$ state, extracted from the energy separation between peak 3 and peak 4 in (a) . (d) The fitting of RIXS curves with three peaks, representing the excitation from $\Gamma_8$ to $\Gamma_6'$ (peak 3A), $\Gamma_8'$(peak 3B), and $\Gamma_7'$ (peak 4). (e) The FWHM values of the fitted peaks extracted from (e) and two fitted peaks in the $J = 5/2$ state. (f) The extracted total CEF split within the $J = 7/2$ state, extracted from the energy separation between peak 3A and peak 4 in (d).

excitation width. That means the peak 3 should present two well-separated excitations, and thus dual-peak fitting is problematic and misleading by assuming $\Gamma_8'$ and $\Gamma_6'$ are located coincidently in energy.

The discussion above inclines that the RIXS line profile of $J = 7/2$ excitations deserves a better analysis than naive dual-peaks fitting, and the $\Gamma_6'$ and $\Gamma_8'$ states of $J = 7/2$ should be distinguishable under the fitting. Therefore, a fitting of $J = 7/2$ excitations with three peaks is also presented in Fig. 4(d-f). The overall fitting quality is significantly improved and the sum of squares (SS) value has been shrunk to one order of magnitude smaller than the dual-peak fitting. More importantly, the fitting details of peaks are now much more reasonable. For instance, the FWHM of every peak is now rather comparable to each other, correcting the errors in the dual peaks fitting that one peak is overwhelmingly broader than the others (Fig. 4(e)). Still, peak 3B, which attributes to the quadruplet $\Gamma_8'$ states ($J = 7/2$), possesses more intensity than peak 3A (doublet $\Gamma_6'$) and peak 4 (doublet $\Gamma_7'$). The fitting-extracted energy split between the $\Gamma_6'$ and $\Gamma_8'$ is about 25 meV, which is also larger than the value of 14 meV reported in Raman scattering. Besides that, the CEF split between the $\Gamma_7'$ and $\Gamma_8'$ is about 65 meV, nearly identical to the Raman scattering result. Together, the fitting gives an overall CEF split of 89.5 meV within the $J = 7/2$ states (Fig. 4(f)). The CEF value of 89.5 meV extracted from our RIXS data is about 10% larger than the value of 82 meV from the Raman experiment. However, it is not necessary to draw a conclusion that either value is more accurate unless the following considerations are clearly resolved.

First, the divergence could be a direct result of the difference between these two experimental techniques. It has also been reported in other research that excitation energy probed by RIXS could be larger than the ones from Raman scattering. As an example, the first-order vibration mode in water's O-H band probed by RIXS shows an apparent blueshift when compared with the result of Raman scattering.[44–46]. Although both techniques are on the basis of scattering, Raman scattering is related to the non-resonant process, while the RIXS relies on energy resonance.

The conflicts may also be intrinsically linked to the less metallic nature of the heavily alloyed Ce/$SmB_6$. Previous magnetic susceptibility measurements and our XAS measurements support the dominance of $4f^1$ valence state in the alloyed compound, and substituting with Sm would not change the lattice configuration of $B_6$ cages surrounding the Ce-site. However, it is noteworthy that CEF is raised from the molecular orbital model, which is highly associated with an insulating picture and would be blurred by the quasiparticle dispersions and enhanced bandwidth. Instead of the insulating $SmB_6$ [47, 48], $CeB_6$ is a Kondo metal[49, 50]. Heavily alloying Ce with Sm would depress the itinerancy in the $CeB_6$, which enhances

the energy scale of CEF. The cooling down of $CeB_6$ makes it more insulating, but larger CEF splitting. This effect could also be realized in the temperature-dependent Raman data in Ref.[35, 51].

## IV.CONCLUSION

In this paper, we precisely depicted the energy scales of CEF symmetries by using high-resolution RIXS. Our result suggests a larger CEF split of 89.5 meV in the $J = 7/2$ states when comparing our findings with a recent Raman spectroscopy work. With respect to the discrepancy, it can't be excluded as a result associated with the alloying with Sm (intrinsic) or the difference of the scattering process (extrinsic). Although further study is necessary to reconcile the dispute between our result with the previous one, our work constitutes a piece of new evidence to the theoretical community and hopefully provides insights into the strongly correlated system with Ce-$4f^1$ basis. As already mentioned, the CEF split ground state symmetry and the framework of CEF energy hierarchy give the basis for comprehending the electronic correlations and the non-trivial topology in the heavy fermion material $Ce_{0.3}Sm_{0.7}B_6$. For example, the value of CEF could signal the bandwidth, itineracy as well as hybridization between $f$-orbital and other bands. Thus, an accurate CEF energy level would put an explicit constraint on the first principle calculation, which would generate a theoretical treatment much closer to the underlying physics.

## ACKNOWLEDGEMENTS

L.M. was supported by the National Natural Science Foundation of China (Grants No. U2032156 and No. 12004071), Natural Science Foundation of Jiangsu Province, China (Grant No. BK20200348), Ministry of Science and Technology of China (Grants No. 2022YFA1405700), and the program of Jiangsu specially-appointed professor. L.A.W. acknowledges the support of the National Science Foundation under Grant No. DMR-2105081. This research used resources of the Advanced Light Source, a U.S. DOE Office of Science User Facility under Contract No. DE-AC02-05CH11231.

* Electronic address: lawray@nyu.edu.cn; Corresponding author
† Electronic address: lmiao@seu.edu.cn; Corresponding author

[1] K. N. Lee and B. Bell, Phys. Rev. B **6**, 1032 (1972).
[2] K. Haule, C.-H. Yee, and K. Kim, Phys. Rev. B **81**, 195107 (2010).
[3] Q. Y. Chen, D. F. Xu, X. H. Niu, R. Peng, H. C. Xu, C. H. P. Wen, X. Liu, L. Shu, S. Y. Tan, X. C. Lai, Y. J. Zhang, H. Lee, V. N. Strocov, F. Bisti, P. Dudin, J.-X. Zhu, H. Q. Yuan, S. Kirchner, and D. L. Feng, Phys. Rev. Lett. **120**, 066403 (2018).
[4] C. K. Barman, P. Singh, D. D. Johnson, and A. Alam, Phys. Rev. Lett. **122**, 076401 (2019).
[5] Q. Yao, D. Kaczorowski, P. Swatek, D. Gnida, C. H. P. Wen, X. H. Niu, R. Peng, H. C. Xu, P. Dudin, S. Kirchner, Q. Y. Chen, D. W. Shen, and D. L. Feng, Phys. Rev. B **99**, 081107 (2019).
[6] D. Hafner, P. Khanenko, E.-O. Eljaouhari, R. Küchler, J. Banda, N. Bannor, T. Lühmann, J. F. Landaeta, S. Mishra, I. Sheikin, E. Hassinger, S. Khim, C. Geibel, G. Zwicknagl, and M. Brando, Phys. Rev. X **12**, 011023 (2022).
[7] T. Komatsubara, N. Sato, S. Kunii, I. Oguro, Y. Furukawa, Y. Ōnuki, and T. Kasuya, Journal of Magnetism and Magnetic Materials **31**, 368 (1983).
[8] E. Zirngiebl, B. Hillebrands, S. Blumenröder, G. Güntherodt, M. Loewenhaupt, J. M. Carpenter, K. Winzer, and Z. Fisk, Phys. Rev. B **30**, 4052 (1984).
[9] F. Steglich, J. Aarts, C. D. Bredl, W. Lieke, D. Meschede, W. Franz, and H. Schäfer, Phys. Rev. Lett. **43**, 1892 (1979).
[10] W. Assmus, M. Herrmann, U. Rauchschwalbe, S. Riegel, W. Lieke, H. Spille, S. Horn, G. Weber, F. Steglich, and G. Cordier, Phys. Rev. Lett. **52**, 469 (1984).
[11] C. Petrovic, P. Pagliuso, M. Hundley, R. Movshovich, J. Sarrao, J. Thompson, Z. Fisk, and P. Monthoux, Journal of Physics: Condensed Matter **13**, L337 (2001).
[12] Y. Ōnuki, Y. Shimizu, M. Nishihara, Y. Machii, and T. Komatsubara, Journal of the Physical Society of Japan **54**, 1964 (1985).
[13] H. Sato, I. Sakamoto, K. Yonemitsu, Y. Ōnuki, T. Komatsubara, Y. Kaburagi, and Y. Hishiyama, Journal of magnetism and magnetic materials **52**, 357 (1985).
[14] A. P. Pikul, U. Stockert, A. Steppke, T. Cichorek, S. Hartmann, N. Caroca-Canales, N. Oeschler, M. Brando, C. Geibel, and F. Steglich, Phys. Rev. Lett. **108**, 066405 (2012).
[15] J. Effantin, J. Rossat-Mignod, P. Burlet, H. Bartholin, S. Kunii, and T. Kasuya, Journal of magnetism and magnetic materials **47**, 145 (1985).
[16] M. Kawakami, S. Kunii, T. Komatsubara, and T. Kasuya, Solid State Communications **36**, 435 (1980).
[17] G. Friemel, Y. Li, A. Dukhnenko, N. Y. Shitsevalova, N. Sluchanko, A. Ivanov, V. Filipov, B. Keimer, and D. Inosov, Nature Communications **3**, 830 (2012).
[18] M. Sera, N. Sato, and T. Kasuya, Journal of Magnetism and Magnetic Materials **63**, 64 (1987).
[19] A. S. Cameron, G. Friemel, and D. S. Inosov, Reports on Progress in Physics **79**, 066502 (2016).
[20] W. Erkelens, L. Regnault, P. Burlet, J. Rossat-Mignod, S. Kunii, and T. Kasuya, in *Anomalous Rare Earths and Actinides* (Elsevier, 1987) pp. 61–63.
[21] S. Nakamura, T. Goto, and S. Kunii, Journal of the Physical Society of Japan **64**, 3941 (1995).
[22] S. Yeo, K. Song, N. Hur, Z. Fisk, and P. Schlottmann, Phys. Rev. B **85**, 115125 (2012).
[23] M. Ciomaga Hatnean, T. Ahmad, M. Walker, M. R. Lees, and G. Balakrishnan, Crystals **10** (2020), 10.3390/cryst10090827.
[24] O. Erten, P.-Y. Chang, P. Coleman, and A. M. Tsvelik,

Phys. Rev. Lett. **119**, 057603 (2017).
[25] A. Koitzsch, N. Heming, M. Knupfer, B. Büchner, P. Portnichenko, A. Dukhnenko, N. Shitsevalova, V. Filipov, L. Lev, V. Strocov, *et al.*, Nature communications **7**, 10876 (2016).
[26] P. Y. Portnichenko, A. Akbari, S. E. Nikitin, A. S. Cameron, A. V. Dukhnenko, V. B. Filipov, N. Y. Shitsevalova, P. Čermák, I. Radelytskyi, A. Schneidewind, J. Ollivier, A. Podlesnyak, Z. Huesges, J. Xu, A. Ivanov, Y. Sidis, S. Petit, J.-M. Mignot, P. Thalmeier, and D. S. Inosov, Phys. Rev. X **10**, 021010 (2020).
[27] L. Miao, C.-H. Min, Y. Xu, Z. Huang, E. C. Kotta, R. Basak, M. S. Song, B. Y. Kang, B. K. Cho, K. Kißner, F. Reinert, T. Yilmaz, E. Vescovo, Y.-D. Chuang, W. Wu, J. D. Denlinger, and L. A. Wray, Phys. Rev. Lett. **126**, 136401 (2021).
[28] Y. Xu, E. C. Kotta, M. S. Song, B. Y. Kang, J. W. Lee, B. K. Cho, S. Liu, T. Yilmaz, E. Vescovo, J. D. Denlinger, L. Miao, and L. A. Wray, Phys. Rev. B **104**, 115118 (2021).
[29] M. Sundermann, K. Chen, H. Yavaş, H. Lee, Z. Fisk, M. Haverkort, L. H. Tjeng, and A. Severing, Europhysics Letters **117**, 17003 (2017).
[30] L. Hu, M. F. Reid, C.-K. Duan, S. Xia, and M. Yin, Journal of Physics: Condensed Matter **23**, 045501 (2011).
[31] P. A. Tanner, C. S. Mak, N. M. Edelstein, K. M. Murdoch, G. Liu, J. Huang, L. Seijo, and Z. Barandiarán, Journal of the American Chemical Society **125**, 13225 (2003).
[32] T. Takahashi, T. Morimoto, T. Yokoya, S. Kunii, T. Komatsubara, and O. Sakai, Phys. Rev. B **52**, 9140 (1995).
[33] S. Horn, F. Steglich, M. Loewenhaupt, H. Scheuer, W. Felsch, and K. Winzer, Zeitschrift für Physik B Condensed Matter **42**, 125 (1981).
[34] B. Lüthi, S. Blumenröder, B. Hillebrands, E. Zirngiebl, G. Güntherodt, and K. Winzer, Zeitschrift für Physik B Condensed Matter **58**, 31 (1984).
[35] M. Ye, H.-H. Kung, P. F. S. Rosa, E. D. Bauer, Z. Fisk, and G. Blumberg, Phys. Rev. Mater. **3**, 065003 (2019).
[36] See Supplemental Material at [URL] for additional information about RIXS data of the $CeB_6$ sample, and the atomic multiplet simulations on Ce-$4f^1$, Sm-$4f^5/4f^6$ configurations. The Supplemental Material also contains Ref. [38].
[37] L. A. Wray, J. Denlinger, S.-W. Huang, H. He, N. P. Butch, M. B. Maple, Z. Hussain, and Y.-D. Chuang, Phys. Rev. Lett. **114**, 236401 (2015).
[38] H. He, L. Miao, E. Augustin, J. Chiu, S. Wexler, S. A. Breitweiser, B. Kang, B. K. Cho, C.-H. Min, F. Reinert, Y.-D. Chuang, J. Denlinger, and L. A. Wray, Phys. Rev. B **95**, 195126 (2017).
[39] K. J. Kormondy, L. Gao, X. Li, S. Lu, A. B. Posadas, S. Shen, M. Tsoi, M. R. McCartney, D. J. Smith, J. Zhou, *et al.*, Scientific reports **8**, 7721 (2018).
[40] P. Tieu, X. Yan, M. Xu, P. Christopher, and X. Pan, Small **17**, 2006482 (2021).
[41] M. Magnuson, S. M. Butorin, J.-H. Guo, A. Agui, J. Nordgren, H. Ogasawara, A. Kotani, T. Takahashi, and S. Kunii, Phys. Rev. B **63**, 075101 (2001).
[42] A. Kotani and S. Shin, Rev. Mod. Phys. **73**, 203 (2001).
[43] S. Souma, H. Kumigashira, T. Ito, T. Sato, T. Takahashi, and S. Kunii, Journal of Electron Spectroscopy and Related Phenomena **114**, 729 (2001).
[44] D. Mariedahl, F. Perakis, A. Späh, H. Pathak, K. H. Kim, C. Benmore, A. Nilsson, and K. Amann-Winkel, Philosophical Transactions of the Royal Society A **377**, 20180164 (2019).
[45] E. J. Jaeschke, S. Khan, J. R. Schneider, and J. B. Hastings, *Synchrotron light sources and free-electron lasers: accelerator physics, instrumentation and science applications* (Springer, 2016).
[46] V. Vaz da Cruz, F. Gel'mukhanov, S. Eckert, M. Iannuzzi, E. Ertan, A. Pietzsch, R. C. Couto, J. Niskanen, M. Fondell, M. Dantz, *et al.*, Nature communications **10**, 1013 (2019).
[47] T. Kasuya, Europhysics Letters **26**, 277 (1994).
[48] J. C. Cooley, M. C. Aronson, Z. Fisk, and P. C. Canfield, Phys. Rev. Lett. **74**, 1629 (1995).
[49] M. Neupane, N. Alidoust, I. Belopolski, G. Bian, S.-Y. Xu, D.-J. Kim, P. P. Shibayev, D. S. Sanchez, H. Zheng, T.-R. Chang, H.-T. Jeng, P. S. Riseborough, H. Lin, A. Bansil, T. Durakiewicz, Z. Fisk, and M. Z. Hasan, Phys. Rev. B **92**, 104420 (2015).
[50] T. Komatsubara, N. Sato, S. Kunii, I. Oguro, Y. Furukawa, Y. Ōnuki, and T. Kasuya, Journal of Magnetism and Magnetic Materials **31**, 368 (1983).
[51] C. Terzioglu, D. A. Browne, R. G. Goodrich, A. Hassan, and Z. Fisk, Phys. Rev. B **63**, 235110 (2001).